

Cross-correlations between 21 cm, X-ray and infrared backgrounds

Huan-Yuan Shan and Bo Qin

National Astronomical Observatories, Chinese Academy of Sciences, Beijing 100012, China;
shanhuany@bao.ac.cn

Received 2008 March 7; accepted 2008 May 6

Abstract The history of the cosmological reionization is still unclear. Two ionizing sources, stars and QSOs, are believed to play important roles during this epoch. Besides the 21 cm signals, the infrared emission from PopIII stars and X-ray photons from QSOs can be powerful probes of the reionization. Here we present a cross-correlation study of the 21 cm, infrared and X-ray backgrounds. The advantage of doing such cross-correlations is that we could highlight the correlated signals and eliminate irrelevant foregrounds. We develop a shell model to describe the 21 cm signals and find that PopIII stars can provide higher 21 cm signals than QSOs. Using the ROSAT data for X-ray and AKARI data for infrared, we predict various cross power spectra analytically and discuss prospects for detecting these cross-correlation signals in future low frequency radio surveys. We find that, although these cross-correlational signals have distinct features, so far, they have been difficult to detect due to the high noise of the soft X-ray and infrared backgrounds given by ROSAT and AKARI.

Key words: cosmology: theory — X-rays: diffuse background — infrared: stars

1 INTRODUCTION

The discovery of the Gunn-Peterson troughs in the spectra of the $z > 6$ QSOs in the SDSS survey indicates that the end of the cosmological reionization probably occurred at $z \sim 6$ (White et al. 2003; Wyithe & Loeb 2004), while integral constraints on the total optical depth from WMAP imply that the reionization began at $z \sim 10$ (Spergel et al. 2007). The history of the reionization is still an open question.

The 21 cm spin-flip transition of HI is the most exciting prospective tracer of the reionization epoch. It is a line transition, so that observations at a given frequency select out a unique slice of the high redshift universe. We can therefore reconstruct a three-dimensional (3D) map of the reionization with the spectral and angular variations of the 21 cm brightness. The epoch of reionization spans the formation of the first luminous sources (e.g. PopIII stars and QSOs) which ionized the surrounding gas. Thus a 3D map may provide an unprecedented view of this epoch. Future low frequency radio surveys, such as LOFAR (Huib 2003), 21CMA (Peterson, Pen & Wu 2006) and MWA (Morales 2006), will help to shed light on this issue from the emission or absorption of the 21 cm photons relative to the CMB.

However, the construction of this type of 3D map is difficult due to the complicated and strong foregrounds. Before the construction of a 3D map, a cross-correlation study between the 21 cm and other signals may help us to obtain further information about the reionization. The emissions from QSOs and PopIII stars can both contribute to the reionization, and also account for a fraction of the present-day Soft X-Ray Background (SXRb) and the Cosmic InfraRed Background (CIRB), respectively. Slosar et al. (2007) have studied the cross-correlation between the 21 cm signals, the IR emission and the SZ effect.

We will use an improved model to describe the 21 cm signals, and then estimate the cross-correlations in this paper.

A population of QSOs at $z > 6$ would produce an early X-ray background. Since the IGM is optically thick to photons with energies $E < E_{\text{max}} = 1.8[(1+z)/15]^{0.5} x_{\text{HI}}^{1/3}$ keV, the soft X-rays with $E < E_{\text{max}}$ would be consumed by neutral hydrogen atoms and contribute to reionization. However, the background of harder X-rays would redshift without absorption and be observed as the SXRb at the present epoch. Assuming that accreting black holes are the main sources of the reionizing photons in the high redshift universe, we estimate their contribution to the present SXRb, and the correlation between the 21 cm emission and the SXRb.

Similarly, the CIRb emitted from stars may also correlate with the 21 cm background. PopIII stars at high redshifts are generally invoked to explain the missing IR flux between $1 \mu\text{m}$ and $2 \mu\text{m}$, with most of the intensity associated with the redshifted Ly α emissions during reionization (Santos et al. 2002). Although PopIII stars can explain the “missing” CIRb, it is difficult to account for all of the missing IR intensity. These include the high efficiency required to convert baryons to stars in first galaxies (Madau & Silk 2005), and limits from deep IR imaging data that suggest a lack of the large population of high-redshift dropouts (Salvaterra & Ferrara 2006). Therefore, we may expect some contributions to the CIRb from sources that have reionized the Universe, though the exact intensity of the CIRb from such sources is yet unknown both theoretically and observationally.

In this paper, we will give predictions of the cross power spectra between the 21 cm signals and the “tracers” (SXRb and CIRb) of reionization discussed above, and examine the prospects for detecting these signals in future low frequency radio observations. Throughout the paper we adopt the Λ CDM cosmology given by WMAP, with $(\Omega_M, \Omega_\Lambda, \sigma_8, h_0) = (0.268, 0.732, 0.776, 0.704)$ (Spergel et al. 2007).

2 TRACERS OF REIONIZATION

Our model is based on a halo approach. The distribution and evolution of the halo population can be described by the Press-Schechter formalism (Press & Schechter 1974)

$$\frac{dn_{\text{halo}}}{dM_{\text{halo}}} = -\sqrt{\frac{\pi}{2}} \frac{\bar{\rho}}{M} \frac{\delta_c(z)}{\sigma^2(M_{\text{halo}})} \frac{d\sigma(M_{\text{halo}})}{dM_{\text{halo}}} \exp\left(-\frac{\delta_c^2(z)}{2\sigma^2(M_{\text{halo}})}\right), \quad (1)$$

where $\bar{\rho}$ is the mean cosmic density, δ_c is the linear overdensity of a perturbation that collapsed and virialized at redshift z , and σ is the linear theory variance of the mass density fluctuation in a sphere of mass $M = 4\pi\bar{\rho}R^3/3$:

$$\sigma^2(M_{\text{halo}}) = \frac{1}{2\pi^2} \int_0^\infty k^2 P(k) |W(kR)|^2 dk, \quad (2)$$

where $W(x) = 3(\sin x - x \cos x)/x^3$ is the Fourier representation of the window function. The power spectrum, $P(k) \propto k^{n_s} T^2(k)$, is normalized by the rms fluctuation on σ_8 . We take the fitting by Bardeen et al. (1986) for the transfer function $T(k)$. The primordial power spectra is assumed to be the Harrison-Zeldovich case where $n_s = 1$.

2.1 SXRb from QSOs

In order to seed the growth of a QSO, it is sufficient that only one halo had formed a low-spin disk that produced a black hole progenitor. Note that if a low-spin object is embedded in an overdense region that eventually becomes a galactic bulge, the black hole progenitor will sink to the center of the bulge by dynamical friction in less than a Hubble time. We assume the central black hole’s minimum mass to be $10^6 M_\odot$, and the ratio between a QSO and its host halo mass $\epsilon = \frac{M_{\text{QSO}}}{M_{\text{halo}}} \sim 10^{-3.2}$ (Haiman & Loeb 1997).

Telfer et al. (2002) gave a UV-X-ray spectrum from a sample of HST QSOs,

$$\epsilon_X(M_{\text{QSO}}, \nu) = 1.3 \times 10^{31} \text{ erg s}^{-1} (\text{Hz})^{-1} \left(\frac{\nu}{\nu_{\text{ion}}} \right)^{-\alpha} \left\{ 1 + \frac{1}{\sqrt{2\pi}\sigma_\lambda} \exp \left[-\frac{(c/\nu - \lambda_\alpha)^2}{\sigma_\lambda^2} \right] \right\} \frac{M_{\text{QSO}}}{2 \times 10^9 M_\odot}, \quad (3)$$

which can be extended into the X-ray regime based on the results of Yuan et al. (1998). Here $\alpha \sim 1.57$, and $\nu_{\text{ion}} = 3.29 \times 10^{15}$ Hz is the Lyman-limit frequency corresponding to the ionization threshold of hydrogen. We include the Ly α emission line centered at $\lambda_\alpha = 912$ Å (Vanden Berk et al. 2001; Telfer et al. 2002) and a line width $\sigma_\lambda = 19$ Å (Vanden Berk et al. 2001). The normalization of this spectrum is appropriate for a $2 \times 10^9 M_\odot$ supermassive black hole accreting at its Eddington rate (Elvis et al. 1994). We can evaluate the mean SXR brightness $J(\nu)$ by

$$J(\nu) = \int dz \frac{dV}{dz d\Omega} \int_{M_{\text{min}}}^{\infty} dM_{\text{halo}} q(z, M_{\text{halo}}) \frac{dn_{\text{halo}}}{dM_{\text{halo}}} \frac{\epsilon_X(M_{\text{halo}}, \nu)}{4\pi D_L^2}, \quad (4)$$

where $q(z, M_{\text{halo}}) = \frac{\int_{t(z)-\tau_X}^{t(z)} \frac{d^2 n_{\text{halo}}}{dm dt'} dt'}{\frac{dn_{\text{halo}}}{dM_{\text{halo}}}}$ is the ratio of halos with survived QSOs to all the halos at redshift z and $\frac{d^2 n_{\text{halo}}}{dM_{\text{halo}} dt'}$ is the approximate halo formation rate. The actual halo formation rate is larger because the halo formation rate ignores the contribution from merging halos. However, collapsed objects are rare at high redshifts, so the merger probability is low. As a result, this formula can be utilized to describe the halo formation rate at high redshift accurately (Haiman & Loeb 1997), and it is also the lower limit of the halo formation rate at lower redshifts. D_L is the luminosity distance, $\tau_X \sim 10^7$ yr is the characteristic age of QSOs (Wyithe & Loeb 2002). Our predicted mean SXR brightness is shown in Figure 1. For comparison, we also plot the upper limits given by various observations.

In order to predict the power spectrum of the SXR, it is necessary to get the X-ray surface brightness distribution in direction θ :

$$I_X(z, M_{\text{halo}}, \nu, \theta) = \frac{1}{4\pi(1+z)^4} \int j_X(R, M_{\text{halo}}, \nu) d\kappa, \quad (5)$$

where $R = \sqrt{D_A^2 \theta^2 + \kappa^2}$ is the radial distance, D_A is the angular diameter distance to the halo, the integration is along the line-of-sight κ , and the emissivity of X-ray photons is determined through

$$j_X(R, M_{\text{QSO}}, \nu) = \frac{\epsilon(M_{\text{QSO}}, \nu) e^{-\frac{R}{l_E}}}{4\pi R^2 l_E}, \quad (6)$$

with the mean free path of photons

$$l_E = (n_H \sigma)^{-1} \sim 0.23 \times \left(\frac{1+z}{10} \right)^{-3} \left[1.34 \left(\frac{13.6}{h\nu} \right)^{2.99} - 0.34 \left(\frac{13.6}{h\nu} \right)^{3.99} \right]^{-1} \text{ kpc}. \quad (7)$$

2.2 CIRB from PopIII Stars

The CIRB from PopIII stars can be evaluated using the method of the previous subsection. We assume PopIII stars can form in halos with virial temperatures $T \geq T_{\text{min}} = 10^4$ K, in which atomic cooling is effective and allows the gas to sink to the center of the potential well and fragment (Barkana & Loeb 2001). This temperature corresponds to a minimum halo mass,

$$M_{\text{halo}} \geq M_{\text{min}} = 0.94 \times 10^8 M_\odot \left(\frac{h}{0.7} \right)^{-1} \left(\frac{\Omega_m}{0.3} \right)^{-\frac{1}{2}} \left(\frac{1+z}{10} \right)^{-\frac{3}{2}} \left(\frac{\mu}{0.6} \right)^{-\frac{3}{2}} \left(\frac{T_{\text{min}}}{10^4 \text{ K}} \right)^{\frac{3}{2}}, \quad (8)$$

where μ is the mean molecular weight ($\mu = 0.6$ for ionized gas and $\mu = 1.2$ for neutral gas).

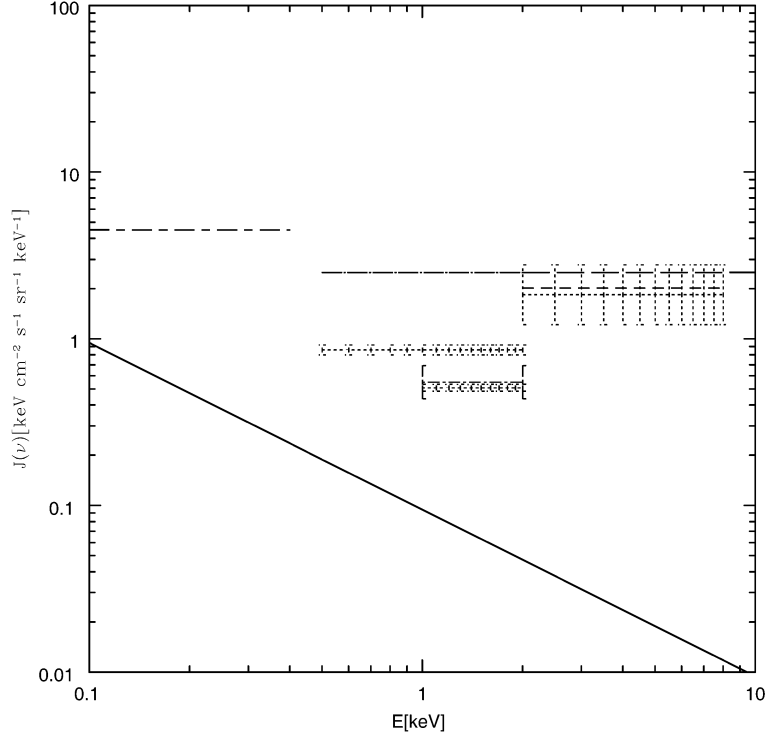


Fig. 1 Comparison of the predicted SXR to the observational upper limits. The observational data are from Wu & Xue (2001). The solid line is the predicted result. The long-dashed line is the observational upper limit in the 2 – 10 keV band (Mushotzky et al. 2000; Giacconi et al. 2001; Tozzi et al. 2001). The short-dashed line is the constraint by Cowie et al. (2002) in the 2 – 8 keV band. The points with error bars and the dot-short-dashed line are the total SXR in the 1 – 2 keV band derived by Miyaji et al. (1998) and Gendreau (1995). The dotted-long-dashed line and the short-dashed-long-dashed line are the upper limits derived by Bryan & Voit (2001) in the 0.5 – 2 keV and 0.1 – 0.4 keV bands. The recent upper limits in the 0.5 – 2 keV, 1 – 2 keV and 2 – 8 keV bands derived by Kim et al. (2007) are shown by the dotted lines.

We take the spectrum of PopIII stars from Santos et al. (2002),

$$\epsilon_{\text{CIRB}}(M_{\text{halo}}, \nu) = M_{\text{stars}} l_{\nu} = \eta \frac{\Omega_b}{\Omega_m} M_{\text{halo}} l_{\nu}, \quad (9)$$

where l_{ν} is the infrared spectrum of a PopIII star. The prefactors $\eta \sim 0.4$ means that 40% of the total mass of a halo can be converted into stellar mass.

For PopIII stars, we assume that the emission of the infrared photons from a halo traces the NFW profile (Navarro et al. 1997),

$$j_{\text{CIRB}}(R, M_{\text{halo}}, \nu) = \frac{N \epsilon_{\text{CIRB}}(M_{\text{halo}}, \nu)}{(R/r_s)(1 + R/r_s)^2}, \quad (10)$$

where r_s is the characteristic length of a halo, and $N = \frac{1}{4\pi r_s^3 [\ln(1+c) - \frac{c}{1+c}]}$ is the normalization factor.

Similarly, following Equation (5), the infrared surface brightness distribution from PopIII stars can be evaluated with the above parameters.

$$I_{\text{CIRB}}(z, M_{\text{halo}}, \nu, \theta) = \frac{1}{4\pi(1+z)^4} \int j_{\text{CIRB}}(R, M_{\text{halo}}, \nu) d\kappa. \quad (11)$$

2.3 21 cm Signals from Neutral Hydrogen

The 21 cm brightness temperature relative to the CMB temperature of a patch in the IGM is (Zaldarriaga, Furlanetto & Hernquist 2004)

$$\delta T = 27 \text{ mK} \frac{T_s - T_{\text{CMB}}}{T_s} (1 + \delta) x_{\text{HI}} \frac{\Omega_b h^2}{0.023} \left(\frac{0.15}{\Omega_m h^2} \frac{1+z}{10} \right)^{1/2}, \quad (12)$$

where T_s and T_{CMB} are the hydrogen spin temperature and the CMB temperature, respectively, δ is the fractional overdensity, and $x_{\text{HI}} = 1 - x_i$ is the neutral fraction.

The ionization fraction x_i at position R for stars and QSOs can be expressed as

$$x_i = \begin{cases} 1, & R < R_{\text{HII}} \\ 0 \text{ or } e^{-R/l_E}, & R > R_{\text{HII}} (\text{stars or QSO}), \end{cases} \quad (13)$$

where R is the radial distance from ionizing sources, R_{HII} is the radius of the HII region. There is no 21 cm emission within the HII region around a radiation source.

The hydrogen spin temperature plays a key role in determining the amplitude of the 21 cm emission or absorption signal against CMB. Due to the presence of the Ly α photons, a strong coupling between the spin temperature (T_s) and the kinetic temperature (T_k) is introduced by the resonance scattering of Ly α photons (the Wouthuysen-Field effect, Field 1958). The spin temperature is given by

$$T_s = \frac{T_{\text{CMB}} + y_\alpha T_\alpha + y_c T_k}{1 + y_\alpha + y_c}, \quad (14)$$

where

$$y_\alpha = \frac{P_{10} T_*}{A_{10} T_k}, \quad y_c = \frac{C_{10} T_*}{A_{10} T_k}. \quad (15)$$

Note that as long as the medium is optically thick to Ly α photons, we would have $T_\alpha = T_k$. Here, $T_* = h_p \nu / k_B \sim 0.0682 \text{ K}$ is the temperature corresponding to the energy difference between the hyperfine levels, $A_{10} = 2.87 \times 10^{-15} \text{ s}^{-1}$ is the spontaneous emission coefficient of the 21 cm line, and $C_{10} = \kappa_{10} n_{\text{H}}$ is the collisional de-excitation rate of the excited hyperfine level. The value of κ_{10} ranges from 2×10^{-14} to $2.5 \times 10^{-10} \text{ cm}^3 \text{ s}^{-1}$ for T in the range 1 – 1000 K (Allison & Dalgarno 1969). The indirect de-excitation rate P_{10} of the hyperfine structure levels is related to the Ly α scattering rate per H atom P_α by $P_{10} = 4P_\alpha/27$ (Field 1958), with $P_\alpha = \int d\nu c n_\nu \sigma_\alpha(\nu)$, where n_ν is the number density of photons per unit frequency and $\sigma_\alpha(\nu)$ is the cross section for Ly α scattering. The scattering rate has been estimated by Madau et al. (1997) as

$$P_\alpha = \int d\Omega \int \frac{J_\nu}{h_p \nu} \sigma_\alpha(\nu) d\nu \sim 8 \times 10^{-11} \text{ s}^{-1} \left(\frac{R}{1 \text{ Mpc}} \right)^{-2} \frac{\nu_\alpha \epsilon_\alpha}{3 \times 10^{46} \text{ erg s}^{-1}}. \quad (16)$$

The kinetic temperature of the gas evolves as

$$\frac{3}{2} n_{\text{H}} k_B \frac{dT_k}{dt} = \dot{E} \quad \dot{E} = \dot{E}_X + \dot{E}_{\text{Ly}\alpha}, \quad (17)$$

where n_{H} is the comoving number density of neutral hydrogen, \dot{E}_X and $\dot{E}_{\text{Ly}\alpha}$ are the X-ray and Ly α heating rates, respectively. For PopIII stars, because few X-ray photons are emitted ($\dot{E}_X \sim 0$), we only

need to consider the Ly α heating. The scattering of Ly α photons can provide a source of heating for the gas. The average relative change in a Ly α photon's energy after being scattered by a hydrogen atom at rest is

$$\left\langle \frac{\Delta E}{E} \right\rangle = -\frac{h\nu_\alpha}{m_{\text{H}}c^2} \approx -10^{-8}, \quad (18)$$

where m_{H} is the mass of the hydrogen atom. It should be noted that this estimate is an approximation which is valid only for $h\nu_\alpha \gg kT_{\text{k}}$. The energy is transferred from photons to atoms at a rate

$$\dot{E}_{\text{Ly}\alpha} = -\left\langle \frac{\Delta E}{E} \right\rangle h\nu_\alpha n_{\text{H}} P_\alpha. \quad (19)$$

Note that this heating rate is proportional to the Ly α scattering rate.

For QSOs, since the scattering of Ly α photons produces a negligible heating rate for the IGM gas, the main heating mechanism should be dominated by X-rays (Wyithe & Loeb 2004). The X-ray heating rate can be written as (Chuzhoy et al. 2006)

$$\dot{E}_{X,\text{tot}} = f_X \int \frac{N_X \epsilon_X(M_{\text{QSO}}, \nu_X) e^{-R/l_E}}{4\pi R^2 l_E} d\nu, \quad (20)$$

where $f_X = 0.9971\{1 - [1 - (1 - x_{\text{HI}})^{0.2663}]^{1.3163}\}$ is the fraction of photon energy being converted into heat, $\Delta\nu_X$ is the frequency interval, N_X is the normalization factor, and $\epsilon_X(M_{\text{QSO}}, \nu_X)$ is QSOs' X-ray spectrum given by Equation (3).

Zaldarriaga et al. (2004) have used a simple model for the 21 cm background. Their model was based on an assumption $T_{\text{s}} \gg T_{\text{CMB}}$ which means that the intergalactic gas has been significantly preheated. However, this is a very strong assumption. The spin temperature T_{s} should be related to the heating rates which are a function of R . Simulations have shown that the 21 cm signals from QSOs should be a shell (Tozzi et al. 2001). Therefore, we now construct a shell model analytically.

The distribution of the 21 cm background of a halo can be written as

$$\delta I(z, M_{\text{halo}}, \theta) = \frac{1}{4\pi(1+z)^4} \int_{R_1}^{R_2} \delta I(z, M_{\text{halo}}, \nu, R) d\kappa, \quad (21)$$

where the integral limits R_1 and R_2 are related to the HII region R_{HII} and HI region R_{HI} , with $R_{\text{HI}} = R_{\text{HII}} + l_E(\nu)$. The mean free path of photons $l_E(\nu)$ is also the thickness of the 21 cm shell, which is the distance that a photon can travel through the neutral medium before it ionizes an atom.

We choose the HII region of a single QSO or PopIII star as its Strömngren sphere

$$\frac{dR_{\text{HII}}}{dt} = 3H(z)R_{\text{HII}} + \frac{3\dot{N}_{\text{ph}}}{4\pi\langle n_{\text{H}} \rangle} - C_{\text{HII}}\langle n_{\text{H}} \rangle\alpha_B R_{\text{HII}}, \quad (22)$$

where $H(z)$ is the Hubble constant at redshift z , $\langle n_{\text{H}} \rangle$ is the mean hydrogen density, \dot{N}_{ph} is the emission rate of the ionizing photons by the source, α_B is the hydrogen recombination coefficient, and C_{HII} is the mean clumping factor of the ionized gas within the HII region. Cosmological simulations indicate that the value of C_{HII} is likely to be 100 (Gnedin & Ostriker 1997). The three terms on the right-hand side of the above equation account for the Hubble expansion, the ionizations by newly produced photons, and the recombination, respectively (Sharpiro & Giroux 1987; Haiman & Loeb 1997). Madau et al. (1997) gave a simple formula,

$$R_{\text{HII}} \approx 10.2 \text{ Mpc} \left(\frac{\dot{N}_{\text{ph}}}{10^{57} \text{ s}^{-1}} \right)^{1/3} \left(\frac{\Omega_b h^2}{0.05} \right)^{-1/2} \left(\frac{1+z}{7} \right)^{-11/6} \Delta z^{1/3}. \quad (23)$$

For an ionization front generated by QSOs, $\dot{N}_{\text{ph}} \sim 6.6 \times 10^{47} \frac{M_{\text{QSO}}}{M_\odot} \text{ s}^{-1}$. For a star forming galaxy, $\dot{N}_{\text{ph}} \sim 3.3 \times 10^{47} \frac{M_{\text{stars}}}{M_\odot} \text{ s}^{-1}$ (Haiman & Loeb 1998). Figure 2 shows the resulting reionization history by stars and QSOs in our model. Apparently, the universe can be completely ionized by stars before $z = 9$.

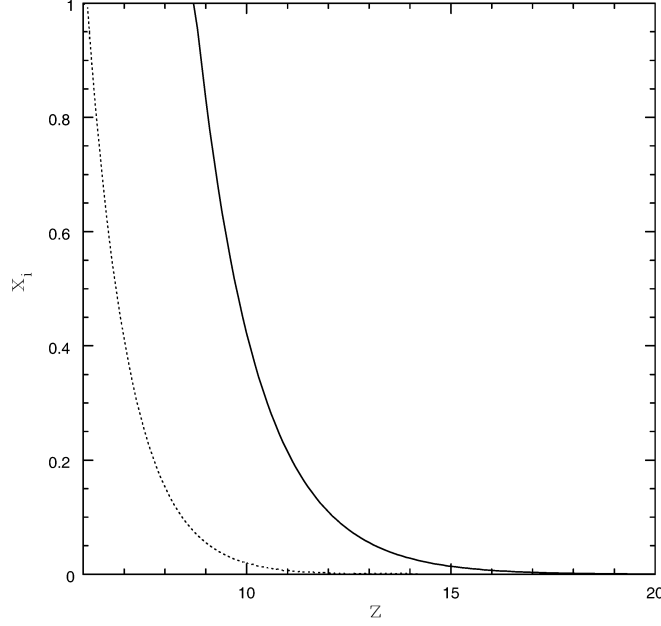


Fig. 2 The global ionization history by stars (solid line) and by QSOs (dotted line) in our model.

3 POWER SPECTRA

Following the halo approach to large scale structure clustering, the angular cross power spectra of the SXRb-21 cm and CIRB-21 cm fluctuation correlations can be separated into the Poisson term C_i^P and the clustering term C_i^C :

$$C_i^P = \int dz \frac{dV}{dz d\Omega} \int dM_{\text{halo}} \frac{dn_{\text{halo}}}{dM_{\text{halo}}} \delta I_{21 \text{ cm}} \delta I_{\text{SXRb/CIRB}}, \quad (24)$$

and

$$C_i^C = \int dz \frac{dV}{dz d\Omega} P_{\text{lin}}(l/D_0, z) \int dM_{\text{halo}} \frac{dn_{\text{halo}}}{dM_{\text{halo}}} b(z, M_{\text{halo}}) \delta I_{21 \text{ cm}} \\ \times \int dM_{\text{halo}} q(z, M_{\text{halo}}) \frac{dn_{\text{halo}}}{dM_{\text{halo}}} b(z, M_{\text{halo}}) \delta I_{\text{SXRb/CIRB}}, \quad (25)$$

where D_0 is the comoving angular diameter distance to a halo of mass M_{halo} at redshift z , $\delta I_{21 \text{ cm}}$ and $\delta I_{\text{SXRb/CIRB}}$ are the Fourier transforms of the 21 cm temperature fluctuation and the SXRb or CIRB brightness fluctuation, respectively, and $b(z, M_{\text{halo}})$ is the bias parameter, for which we use the analytic prescription of Mo & White (1996). The Fourier transform of the background brightness distribution $I(z, M_{\text{halo}}, \theta)$ in the case of spherical symmetry for the distribution in a halo is determined by

$$I_l(z, M_{\text{halo}}) = 2\pi \int I(z, M_{\text{halo}}, \theta) J_0(l\theta) \theta d\theta, \quad (26)$$

where $J_0(l\theta)$ is the cylindrical Bessel function.

Figure 3 shows the auto power spectra of the 21 cm signals from stars and QSOs at different redshifts. Apparently, PopIII stars can provide higher auto power spectra (about one order of magnitude

higher) than QSOs. Here, we do not consider lower redshifts because the stars can ionize the whole universe before $z = 9$ in our model, which means that there would be no 21 cm emission at lower redshifts.

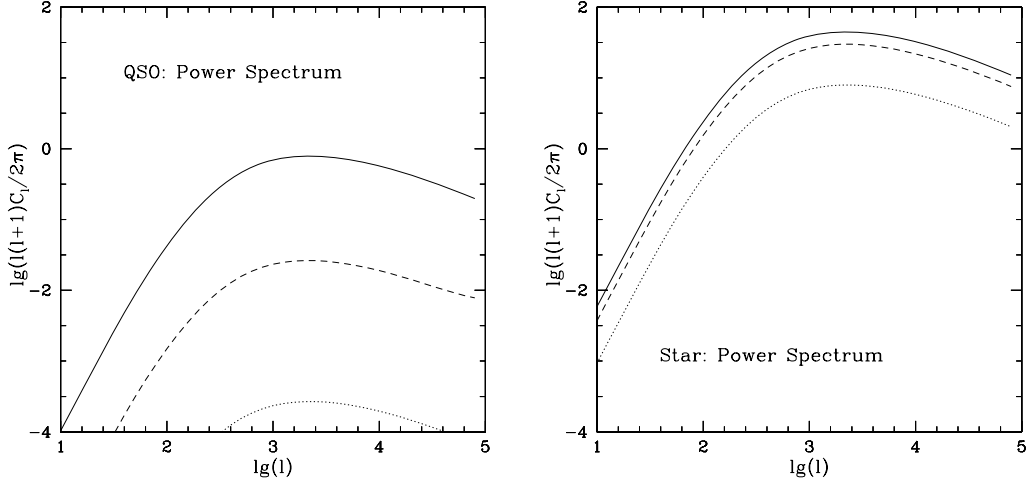


Fig. 3 Angular power spectra of the 21 cm signals from QSOs and stars at redshift $z = 10$ (solid line), $z = 11$ (dashed line), and $z = 12$ (dotted line).

Figure 4 shows the auto power spectra of the SXRb, CIRB and the redshifted 21 cm signals and their cross power spectra. We choose the SXRb at 1 keV, CIRB at $4 \mu\text{m}$, and 21 cm signal at $z = 10$. On large scales, the 21 cm signals are correlated with the SXRb and CIRB. However, on small scales, they are anti-correlated. This means that on scales smaller than the Strömgren sphere of the host halo, QSOs and PopIII stars can emit X-ray or infrared photons, but there is no 21 cm emission.

Finally, we calculate the correlation coefficient as:

$$r_{\text{coll}}(l) = \frac{C_l^{21 \text{ cm} - I}}{\sqrt{C_l^{21 \text{ cm} - 21 \text{ cm}} C_l^{I - I}}}, \quad (27)$$

which quantitatively indicates the strength of the cross-correlation. Here I denotes SXRb or CIRB. Figure 5 shows the correlation coefficient. The cross-over scale of the correlation coefficient for 21 cm-SXRb or 21 cm-CIRB is $l \sim 1000$ or 2512 . Such an l corresponds to about 10 or 5 Mpc which is the characteristic radius of the Strömgren sphere of QSOs or stars at redshift $z = 10$.

4 DETECTABILITY

We now examine the prospects for detecting the cross power spectra of 21 cm-SXRb and 21 cm-CIRB with the future low-frequency survey LOFAR, and the existing X-ray observation ROSAT and the infrared survey AKARI. Following the standard treatment, we estimate various auto power spectra ($I - I$ denotes SXRb-SXRb, CIRB-CIRB, and 21 cm-21 cm) and cross power spectra ($I - J$ denotes SXRb-21 cm, and CIRB-21 cm) as

$$\Delta C_l^{I-I} = \sqrt{\frac{2}{(2l+1)\Delta l f_{\text{sky}}^I}} C_l^{I-I, \text{tot}}, \quad (28)$$

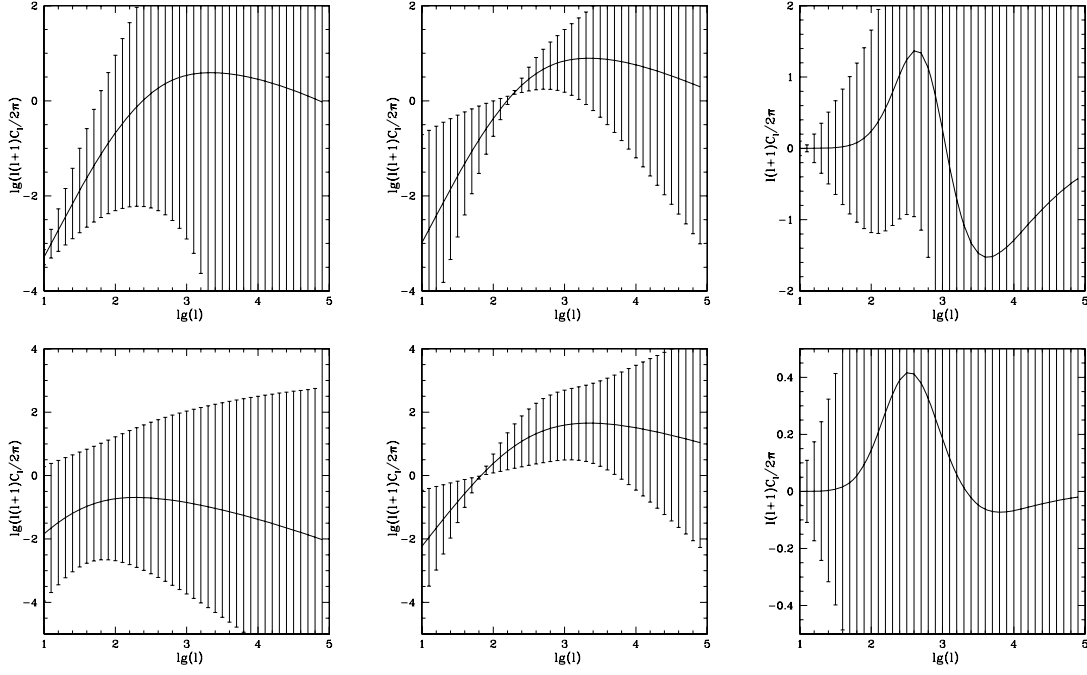


Fig. 4 The power spectra with noise estimate (LOFAR for 21 cm, ROSAT for X-ray and AKARI for CIRB). Top: from left to right, auto power spectra of SXRB (1keV) from QSOs, auto power spectra of 21 cm fluctuation from QSOs at $z = 10$ and cross power spectra between them. Bottom: from left to right, auto power spectra of CIRB ($4 \mu\text{m}$) from PopIII stars, auto power spectra of 21 cm fluctuation from PopIII stars at $z = 10$ and cross power spectra between them.

and

$$\Delta C_l^{I-J} = \sqrt{\frac{1}{(2l+1)\Delta l f_{\text{sky}}^I}} \left[(C_l^{I-J})^2 + C_l^{I-I,\text{tot}} C_l^{J-J,\text{tot}} \right]^{1/2}, \quad (29)$$

where f_{sky}^I is the sky coverages of the LOFAR, ROSAT, and AKARI surveys, $\Delta l \sim 1$ is the bin width, and C_l^{tot} denotes all contributions to the measured power spectra that are essentially composed of true signals and the detector noise, $C_l^{\text{tot}} = C_l + C_l^{\text{noise}}$.

For the 21 cm observations (LOFAR), we follow Zaldarriaga, Furlanetto & Hernquist (2004) to estimate the noise of the 21 cm signals' power spectra:

$$\left(\frac{l^2 C_l^{\text{noise}}}{2\pi} \right)^{1/2} \sim 12 \text{ mK} \frac{T_{\text{sys}}}{200 \text{ K}} \frac{0.1}{f(l)} \left(\frac{0.4 \text{ MHz}}{\Delta\nu} \frac{1 \text{ month}}{t_0} \right)^{1/2}, \quad (30)$$

in which $T_{\text{sys}} \sim 200 \text{ K}$, $\Delta\nu \sim 0.4 \text{ MHz}$, $t_0 \sim 1 \text{ month}$, and $f(l) = f_{\text{cover}} \frac{l_{\text{max}}}{l}$. For LOFAR, $f_{\text{cover}} \sim 0.016$ and $l_{\text{max}} \sim 5000$.

For the X-ray and infrared observations (ROSAT and AKARI), the instrumental noise per mode can be modeled as

$$C_l^{\text{noise}} = w^{-1} \exp[\theta^2(\nu)l(l+1)], \quad (31)$$

where we have assumed that the experimental beam is Gaussian with a width $\theta^2(\nu)$ [FWHM = $(8 \lg 2)^{1/2} \theta(\nu)$], and the noise level per pixel is

$$w^{-1/2} = \frac{\text{FWHM} \sigma_{\text{noise}}}{\sqrt{\eta}}, \quad (32)$$

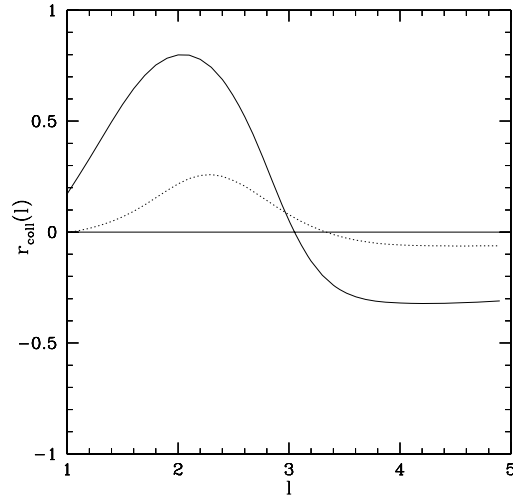


Fig. 5 The correlation coefficients for 21 cm-SXRB (solid line) and 21 cm-CIRB (dotted line) at $z = 10$.

where FWHM is the full width of half maximum, σ_{noise} is the pixel noise, and $\eta = \frac{\text{FWHM}^2 \times N}{4\pi}$ is a dimensionless quantity and N is the number of pixels for a sky map. We list these parameters in Table 1.

Table 1 Observation parameters for ROSAT (HRI) and AKARI (Jeong et al. 2006).

| Obs. | FWHM (arcsec) | f_{sky} | $w^{-1/2}$ (mJy sr $^{-1}$) |
|-------|---------------|------------------|------------------------------|
| ROSAT | 2 | 1 | 0.16 |
| AKARI | 10 | 1 | 20 |

Although the errors of the auto power spectra of the 21 cm fluctuation are small at $l \sim 1000$ (see Fig. 4), the errors of cross power spectra are too large for the signals to be detected. This is mainly because of the high noise of the auto power spectra of the SXRB and CIRB given by ROSAT and AKARI. This means the constraints are mainly due to the SXRB and CIRB. Improving the 21 cm signals by SKA would not help too much. It is unlikely that one can acquire meaningful information about the cross power spectra that are significantly below the noise levels of our interested range of multipoles.

5 CONCLUSIONS AND DISCUSSION

The warm neutral hydrogen outside the HII regions surrounding both QSOs and PopIII stars is expected to emit 21 cm signals. Meanwhile, QSOs and PopIII stars have quite different spectral features. Some photons from them will redshift without absorption and may account for a fraction of the present-day SXRB and CIRB. A cross-correlation study of the 21 cm, SXRB and CIRB may help us understand the history of the reionization epoch. We have presented a simple, physically motivated model to describe the SXRB from QSOs and the CIRB from PopIII stars, and compare the predicted SXRB with observational upper limits (see Fig. 1). We choose the HII region of a QSO or PopIII star as its Stromgren sphere, and describe the 21 cm emission with a shell model. Our results indicate that PopIII stars play a more important role in the reionization history than QSOs (see Fig. 2).

Our auto power spectra results predict that PopIII stars can provide higher 21 cm signals than QSOs (see Fig. 3). Although the auto power spectra detection of 21 cm radio, infrared and X-ray emission can be used to explore the reionization history, the deduction of the complex foregrounds is always a big challenge. The cross-correlation study could avoid such a problem and be used for probing the reionization epoch directly. We find that on large scales, the 21 cm and SXRb (or 21 cm and CIRb) are correlated because they both trace density fluctuations. However, on scales smaller than the bubble size, they are anti-correlated. The cross-over scale can be used to determine the characteristic size of the HII regions of QSOs and PopIII stars.

Applying our algorithm to the future low frequency survey LOFAR, and the existing X-ray surveys ROSAT and AKARI, we find that although the auto power spectra of the 21 cm signals could be detected by LOFAR, the cross-correlations of 21 cm-SXRb and 21 cm-CIRb are still beyond our detection limit. This is due to the high noise of the auto power spectra of the SXRb and CIRb given by ROSAT and AKARI, as shown in our Figure 4. Therefore, future X-ray and infrared surveys with better FWHM and sensitivities are required for our detection of the cross-correlations.

Acknowledgements We thank Xiang-Ping Wu for helpful discussions, and an anonymous referee for comments. This work was partially supported by a CAS grant KJCX3-SYW-N2.

References

- Allison, A. C., & Dalgarno, A. 1969, *ApJ*, 158, 423
 Bardeen, J. M., Bond, J. R., Kaiser, N., & Szalay, A. S. 1986, *ApJ*, 304, 15
 Barkana, R. A., & Loeb, A. 2001, *Physics Reports*, 349, 125
 Bromm, V., Kudritzki, R. P., & Loeb, A. 2001, *ApJ*, 552, 464
 Bryan, G. L., & Voit, G. M. 2001, *ApJ*, 556, 590
 Chuzhoy, L., Alvarez, M., & Shapiro, P. 2006, *ApJ*, 648, L1
 Ciardi, B., & Madau, P. 2003, *ApJ*, 596, 1
 Cowie, L. L., et al. 2002, *ApJ*, 566, L5
 Dijkstra, M., Haiman, Z., & Loeb, A. 2004, *ApJ*, 613, 646
 Elvis, M., et al. 1994, *ApJS*, 95, 1
 Field, G. B. 1958, *Proc. IRE*, 46, 240
 Field, G. B. 1959, *ApJ*, 129, 525
 Furlanetto, S., Sokasian, A., & Hernquist, L. 2004, *MNRAS*, 347, 187
 Gendreau, K. C., et al. 1995, *PASJ*, 47, L5
 Giacconi, R., et al. 2001, *ApJ*, 551, 624
 Gnedin, N. Y. & Ostriker J. P. 1997, *ApJ*, 486, 581
 Haiman, Z., & Loeb, A. 1997, *ApJ*, 483, 21
 Haiman, Z., & Loeb, A. 1998, *ApJ*, 503, 505
 Huub, R. 2003, *NewAR*, 47, 405
 Jeong, W-S., Pearson, C. P., Lee, H.-M., Pak, S., & Nakagawa, T. 2006, *MNRAS*, 369, 281
 Kim, M., Wilkes, B. J., Kim, D., et al. 2007, *ApJ*, 659, 29
 Madau, P., Meiksin, A., & Rees, M. J. 1997, *ApJ*, 475, 429
 Madau, P., & Silk, J. 2005, *MNRAS*, 359, L37
 Matsuhara, T., et al. 2006, *Publ. Astron. Soc. Jap.*, 58,4
 Miyaji, T., et al. 1998, *A&A*, 334, L13
 Mo, H.-J., & White, S. D. M. 1996, *MNRAS*, 282, 347
 Morales, M. F. 2006, *ASPC*, 345, 452
 Moretti, A., Campana, S., Lazzati, D., & Tagliaferri, G. 2003, *ApJ*, 588, 696
 Mushotzky, R., Cowie, L. L., Barger, A. J., & Arnaud, K. A. 2000, *Nature*, 404, 459
 Navarro, J. F., Frenk, C. S., & White, S. D. M. 1997, *ApJ*, 490, 493
 Oh, S. P. 2001, *ApJ*, 553, 499
 Peterson, J. B., Pen, U-L, & Wu, X. 2006, *ASPC*, 345, 441
 Press, W. H. & Schechter, P. 1974, *ApJ*, 187, 425

- Rhook, K. J., & Haehnelt, M. G. 2006, *IAUJD*, 7E, 43
- Rybicki, G.B. & Lightman, A. P. 1979, *Radiative Processes in Astrophysics* (New York: Wiley), 288
- Salvaterra, R. & Ferrara, A. 2006, *MNRAS*, 367, L11
- Spergel, D. N., Bean, R., Dore, O., et al. 2007, *ApJS*, 170, 377
- Santos, M., Bromm, V., & Kamionkowski, M. 2002, *MNRAS*, 336, 1082
- Scott, D. & Rees, M. J. 1990, *MNRAS*, 247, 510
- Shaver, P. A., Windhorst, R. A., Madau, P., & de Bruyn, A. G. 1999, *A&A*, 345, 380
- Shapiro, P. & Giroux, M. L. 1987, *ApJ*, 321, L107
- Slosar, A., Cooray, A., & Silk, J. 2007, *MNRAS*, 377, 168
- Telfer, R. C., Zheng, W., Kriss, G. A., & Rees, M. J. 2002, *ApJ*, 565, 773
- Tozzi, P., Madau, P., Meiksin, A., & Davidsen, A. F. 2000, *ApJ*, 528, 597
- Tozzi, P., et al. 2001, *ApJ*, 562, 42
- Vanden Berk, D. E., et al. 2001, *AJ*, 122, 549
- White, R. L., Becker, R. H., Fan, X., & Strauss, M. A. 2003, *AJ*, 126, 1
- Wu, X-P., & Xue, Y-J. 2001, *ApJ*, 560, 544
- Wyithe, J. S. B., & Loeb, A. 2002, *ApJ*, 581, 886
- Wyithe, J. S. B., & Loeb, A. 2004, *ApJ*, 610, 117
- Yuan, W., Brinkmann, W., Siebert, J., & Voges, W. 1998, *A & A*, 330, 108
- Zaldarriaga, M., Furlanetto, S., & Hernquist, L. 2004, *ApJ*, 608, 622